JHEP

Published for SISSA by Springer

Received: August 30, 2012
Revised: October 5, 2012
Accepted: October 13, 2012
Published: November 12, 2012

$\mathrm{t\bar{t}}W^{\pm}$ + $\mathrm{t\bar{t}}Z$ hadroproduction at NLO accuracy in QCD with Parton Shower and Hadronization effects

M. V. Garzelli,[a] **A. Kardos,**[b] **C. G. Papadopoulos**[c,d] **and Z. Trócsányi**[b]

[a] *Laboratory for Astroparticle Physics, University of Nova Gorica, SI-5000 Nova Gorica, Slovenia*

[b] *Institute of Physics and MTA-DE Particle Physics Research Group, University of Debrecen, H-4010 Debrecen P.O.Box 105, Hungary*

[c] *Institute of Nuclear Physics, NCSR Δημόκριτος, GR-15310 Athens, Greece*

[d] *CERN, TH-Unit, CH-1211 Geneva 23, Switzerland*

E-mail: garzelli@mi.infn.it, kardos.adam@science.unideb.hu, costas.papadopoulos@cern.ch, Zoltan.Trocsanyi@cern.ch

Abstract: We present theoretical predictions for the hadroproduction of $\mathrm{t\bar{t}}W^{+}$, $\mathrm{t\bar{t}}W^{-}$ and $\mathrm{t\bar{t}}Z$ at LHC as obtained by matching numerical computations at NLO accuracy in QCD with Shower Monte Carlo programs. The calculation is performed by `PowHel`, relying on the `POWHEG-BOX` framework, that allows for the matching between the fixed order computation, with input of matrix elements produced by the `HELAC-NLO` collection of event generators, and the Parton Shower evolution, followed by hadronization and hadron decays as described by `PYTHIA` and `HERWIG`. We focus on the dilepton and trilepton decay channels, studied recently by the CMS Collaboration.

Keywords: QCD Phenomenology, NLO Computations

ArXiv ePrint: 1208.2665

doi:10.1007/JHEP11(2012)056

JHEP11(2012)056

Contents

JHEP11(2012)056

1 Introduction

The hadroproduction of $t\bar{t}$-pairs in association with vector bosons is one of the key processes to constrain top quark properties, in particular top couplings, and to detect if anomalies, possibly related to physics beyond the Standard Model (SM), can manifest themselves. Furthermore, it can be considered a background process for new physics searches. In particular, the dilepton decay channel with two same-sign leptons, accompanied by missing energy and jets, is a relatively rare channel in the SM, but largely exploited in recent supersymmetry searches [1]. From the experimental point of view, these studies are becoming feasible thanks to the increasing amount of data collected at LHC, that has already reached an integrated luminosity large enough to permit the disentangling of $t\bar{t}$ + V signals over other SM backgrounds [2]. Such an investigation can certainly benefit from high accuracy theoretical tools, involving the inclusion of radiative corrections, at least in QCD, and the matching to Parton Shower (PS) approaches.

The aim of this paper is to provide predictions for $t\bar{t} + V$ production (with $V = W^+$, W^-, Z) at LHC at both NLO and NLO + PS accuracy. In case of NLO we also include uncertainties due to factorization and renormalization scale variation, always assumed equal one to each other in this work. This is achieved by `PowHel`, an event generator relying on the `POWHEG-BOX` [3] computer framework designed for matching predictions at NLO accuracy in QCD to a PS evolution, according to the POWHEG method [4, 5]. We use as input matrix elements that we compute through codes available in the `HELAC-NLO` package [6]. With such an input, the `POWHEG-BOX` is capable to make predictions at both NLO accuracy, and at NLO accuracy matched to a PS evolution. We especially concentrate on the $\sqrt{s} = 7$ and 8 TeV energies, but the approach can easily be extended to other ones (and to other colliders). By means of this same framework we were already able to produce predictions

for other processes ($t\bar{t}$, $t\bar{t}\,j$, $t\bar{t}\,H/A$) at the same accuracy, which can be considered a good test of its robustness [7–10]. So far, we also presented some theoretical results on $t\bar{t}\,Z$ production itself, at NLO accuracy [11], and a phenomenological study limited to its decay channel in six jets plus missing energy, at NLO + PS accuracy [12].

This paper is new with respect to our previous ones, since here for the first time we produce predictions for $t\bar{t}\,W^{\pm}$ hadroproduction, and we concentrate on the (semi)leptonic decay channels of $t\bar{t}\,Z$, the same channels that are nowadays preferred by the experimental collaborations, as much cleaner signals can be obtained with respect to the fully hadronic decay one. The $t\bar{t}\,W^{\pm}$ hadroproduction has already been recently investigated by `MCFM` at the NLO accuracy in QCD [13]. Our study provides a completely independent confirmation of their results at the parton level, with which we found agreement within the quoted uncertainties. Furthermore, we give predictions for the first time for this same process at the hadron level, by matching the NLO predictions to the `PYTHIA` [14] and `HERWIG` [15] Shower Monte Carlo (SMC) programs, describing PS emissions, hadronization and hadron decays.

The paper is organized as follows. In section 2.1 we provide a short description of the general computing framework, and details on the particular issues we had to face for the implementation of the $t\bar{t}\,V$ specific processes. In section 2.2 we quote our results at NLO accuracy, and we show the checks we did to ensure that the matching between the NLO computation and the PS algorithm is implemented in a correct way. In section 3 we describe the phenomenological studies we performed at the hadron level and we show predictions for differential distributions both at the inclusive level and in the same exclusive selection channels considered by the CMS Collaboration in their data analysis. In particular, our predictions turn out to be compatible with the experimental data in both the trilepton and the dilepton channels, as recorded in the recently published data analysis at 7 TeV. Finally, in section 4 we draw our conclusions with mention to future refinements of this computation.

2 Theoretical framework

2.1 Implementation

We address the problem of matching $t\bar{t}\,V$ ($V = Z,\ W^{\pm}$) production at NLO level to PS programs, to this end the POWHEG approach [4, 5] was chosen as implemented in `POWHEG-BOX` [3]. While details on the implementation of $t\bar{t}\,Z$ in this framework were recorded in our previous papers [11, 12], the following ingredients, needed by `POWHEG-BOX`, were provided in case of $t\bar{t}\,W^{\pm}$ hadroproduction:

- The phase space corresponding to three massive particles in the final state was provided in full analogy with our previous computations of the $t\bar{t}\,Z$ and $t\bar{t}\,H$ processes at the same accuracy [8, 12].
- The Born and real-emission matrix elements corresponding to the $q\bar{q}'\,t\bar{t}\,W^{\pm} \to 0$ and $q\bar{q}'\,t\bar{t}\,W^{\pm}\,g \to 0$ processes, respectively, with $q, q' \in \{u, d, c, s\}$, were provided by `HELAC-NLO` [6].
- The finite part of the virtual amplitudes was computed by `HELAC-1LOOP` [16] for the $q\bar{q}'\,t\bar{t}\,W^{\pm} \to 0$ processes.

JHEP11(2012)056

- At both tree- and one-loop-level the remaining matrix elements were obtained by crossing.

- The spin- and color-correlated Born squared matrix elements were also provided by HELAC-NLO, in particular HELAC-Dipoles [17].

The PowHel (= POWHEG-BOX + HELAC-NLO) code implemented this way is capable of generating Les Houches Events (LHE's), including up to first radiation emission, for both $t\,\bar{t}\,W^+$ and $t\,\bar{t}\,W^-$ with on-shell t-quarks and vector bosons. A selection between $t\,\bar{t}\,W^+$ and $t\,\bar{t}\,W^-$ production can simply be achieved by setting the Wmode keyword in the input card to ± 1.

In order to make comparison with the available NLO predictions [13], we had to use a non-diagonal CKM matrix in the calculation. We thus extended HELAC-1LOOP in this respect. This process can then be considered the first one, among those computed with HELAC-1LOOP, where a non-diagonal CKM matrix was used. A check of the correctness of the implementation was provided by comparing our results with those already available in literature (see next subsection), obtained in the same non-diagonal conditions. We make available the PowHel implementation, where the user has the possibility of switching from a diagonal CKM matrix to the non-diagonal one by specifying a positive value of the sin2cabibbo keyword in the input card, which declares $\sin^2\theta_C$.

2.2 Results at NLO accuracy and checks

In order to assess the correctness of the implementation, a standard set of checks we are used to doing on the PowHel implementation of any new process, was performed also in this case. The consistency between the real emission matrix elements, the Born part, and the real counterterms automatically computed according to the FKS subtraction scheme [18], was checked by investigating the behavior of these terms in all kinematically degenerate regions of phase space. The original and crossed matrix elements computed by PowHel were checked against those provided by HELAC-Phegas and HELAC-1LOOP standalone in various randomly chosen phase space points. As for $t\,\bar{t}\,W^\pm$, the Born results were checked against MCFM [19, 20], and the NLO ones against the predictions quoted in ref. [13], using the same set of parameters mentioned therein and $\sin^2\theta_C = 4.9284\cdot 10^{-2}$, as in the default version of MCFM. In all cases we found full agreement. We also compute NLO $t\,\bar{t}\,W^\pm$ cross-sections at LHC for a different static central scale choice, by considering the interval $[\mu_0/2,\, 2\mu_0]$ centered around $\mu_0 = m_t + m_V/2$, and the following set of parameters: $\sqrt{s} =$ 7 and 8 TeV, the CTEQ6.6M PDF set with a 2-loop running α_s and 5 active flavours, taken from LHAPDF [21], $m_b = 0$, whereas as for heavy particle masses, the latest available values provided by the PDG [22], i.e. $m_t = 173.5\,\text{GeV}$, $m_W = 80.385\,\text{GeV}$ and $m_Z = 91.1876\,\text{GeV}$, were adopted. For the whole calculation a non-diagonal CKM-matrix was used, in the first two families, with $\sin^2\theta_C = 4.9284\cdot 10^{-2}$. The renormalization and factorization scales were fixed to μ_0. The predictions for the total NLO cross-sections in these conditions are shown in table 1. The considered scale choice turned out to provide a flatter scale dependence with respect to the case $\mu_0 = m_t$, as can be understood by comparing the results quoted in table 1 to those provided in ref. [13].

JHEP11(2012)056

	$\sqrt{s}$ (TeV)	μ	$\sigma^{\rm LO}$ (fb)	$\sigma^{\rm NLO}$ (fb)	$\mathcal{K}$-fact.
$\mathrm{t\,\bar{t}}\,W^+$	7	$\mu_0/2$	121.8(1)	114.3(1)	1.13
		μ_0	93.1(1)	104.7(1)	
		$2\mu_0$	72.7(1)	93.8(1)	
	8	$\mu_0/2$	159.3(1)	156.2(2)	1.16
		μ_0	122.9(1)	142.6(2)	
		$2\mu_0$	96.7(1)	127.5(1)	
$\mathrm{t\,\bar{t}}\,W^-$	7	$\mu_0/2$	46.7(1)	46.9(1)	1.20
		μ_0	35.6(1)	42.6(1)	
		$2\mu_0$	27.8(1)	38.0(1)	
	8	$\mu_0/2$	64.1(1)	67.1(1)	1.23
		μ_0	49.4(1)	60.5(1)	
		$2\mu_0$	38.9(1)	53.9(1)	
$\mathrm{t\,\bar{t}}\,Z$	7	$\mu_0/2$	141.6(1)	149.4(2)	1.32
		μ_0	103.5(1)	136.9(1)	
		$2\mu_0$	77.8(1)	120.8(1)	
	8	$\mu_0/2$	209.5(1)	224.9(4)	1.34
		μ_0	153.9(1)	205.7(2)	
		$2\mu_0$	116.2(1)	181.7(2)	

Table 1. `PowHel` predictions for the inclusive $\mathrm{t\,\bar{t}}\,W^+$, $\mathrm{t\,\bar{t}}\,W^-$ and $\mathrm{t\,\bar{t}}\,Z$ cross-sections at LO and NLO QCD accuracy at LHC for $\sqrt{s} = 7$ and 8 TeV, for various static scale choices, centered around $\mu_0 = m_t + m_V/2$, with $V = W$ for the $\mathrm{t\,\bar{t}}\,W^\pm$ cases and Z for the $\mathrm{t\,\bar{t}}\,Z$ one. The statistical uncertainties of our simulations are shown in parentheses.

Although the K-factor associated to the $\mathrm{t\,\bar{t}}\,W^\pm$ process is close to one, it is also informative to compare NLO differential cross-sections to those obtained from the LHE's, which checks the correctness of the matching procedure. Sample distributions can be found in figures 1 and 2, where the transverse momenta and the rapidities of both the t-quark and the $\mathrm{t\bar{t}}$-pair are shown in case of $\mathrm{t\,\bar{t}}\,W^+$ and $\mathrm{t\,\bar{t}}\,W^-$, respectively, together with the ratio of the predictions from the LHE's to the NLO ones. The agreement between the NLO and the LHE distributions is quite remarkable, as can be seen from the two rapidity plots and from the $p_\perp$distribution of the t-quark. The small deviation visible in the $p_{\perp,\mathrm{t}}$ tail is within the increased statistical uncertainty in that region, also plotted in the lower inset of each panel. For the $p_{\perp,\mathrm{t\bar{t}}}$ distribution the agreement is within 5 % up to $\simeq 220$ GeV, but worsens in the high momentum tail. We attribute this increasing difference to the increasing K-factor that reaches 2 around 400 GeV (also depicted in the lower panel of the plot). This 10 % deviation however, is well within the NLO scale dependence, as seen from the upper panel, where the uncertainty band, corresponding to a scale-variation in the $[\mu_0/2, 2\mu_0]$ interval, is shown as well.

Differential K-factors and the comparison between NLO and LHE distributions in case of the $\mathrm{t\,\bar{t}}\,Z$ process can be found in ref. [11, 12]. The effect of $\mathrm{t\bar{t}}\gamma^*$-production and γ^*-Z interference is left for later publication.

JHEP11(2012)056

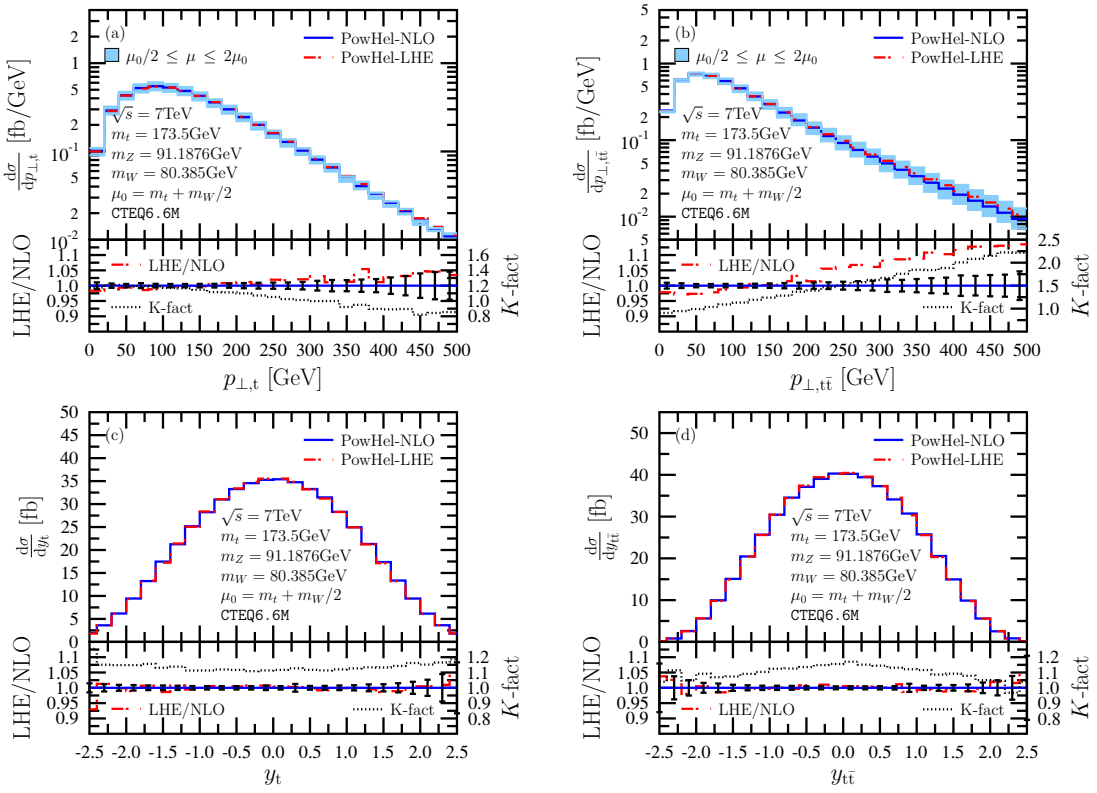

Figure 1. Comparison between differential distributions at NLO accuracy (solid line) and from the LHE's (dashed line), in case of $t\bar{t}W^+$ production. As sample distributions, the transverse momentum and rapidity distributions are shown for the t-quark and for the $t\bar{t}$-pair. In the lower panels the red dash-dotted line corresponds to the LHE/NLO ratio, whereas the differential K-factor (NLO/LO) is depicted with a dotted line. The error-bars refer to the statistical uncertainties on the LHE/NLO ratio. In case of transverse momentum distributions, the scale dependence is also superimposed as a light-blue band, which represents a scale variation between $\mu_0/2$ and $2\mu_0$.

3 Phenomenology

3.1 PowHel and SMC setup

For our phenomenological studies the following parameters were adopted in `PowHel`: the `CTEQ6.6M` PDF set, with a 2-loop running α_s, $m_t = 172.5\,\text{GeV}$, $m_W = 80.385\,\text{GeV}$, $m_Z = 91.1876\,\text{GeV}$, $\sin^2\theta_C = 4.9284 \cdot 10^{-2}$. The renormalization and factorization scales were fixed to $\mu_R = \mu_F = m_t + m_V/2$. Although the value of m_t is different from the most recent measurements at the LHC and also from that used in our NLO comparisons, it was also used in ref. [13] and in several measurements performed by the LHC experiments so far.

The `PowHel` code provides collection of LHE's of two kinds: Born-like events, and events including first radiation emission. According to the POWHEG method, this emission is SMC independent. Further emissions can be simulated by simply showering the events by SMC programs, under the condition that the first emission remains the hardest. We consider the last fortran version of both the `PYTHIA` (6.426) and `HERWIG` (6.520) SMC with their default tunes, providing a virtuality-ordered and an angular-ordered PS, respectively.

JHEP11(2012)056

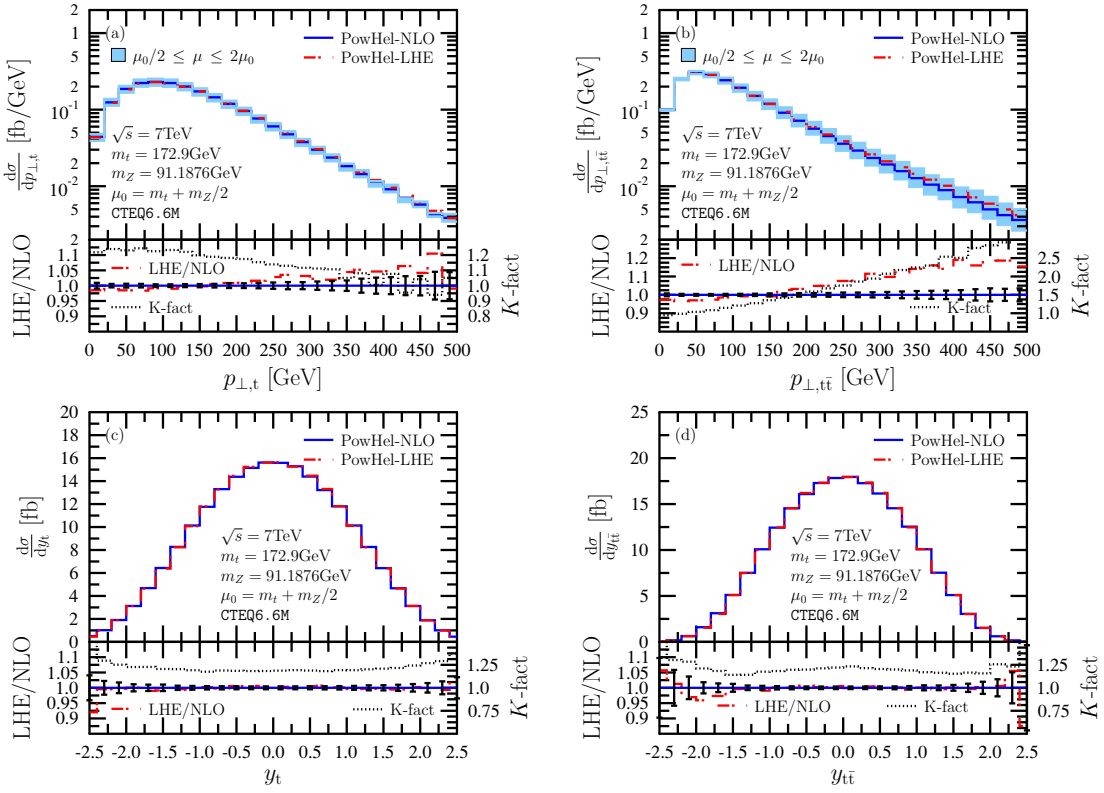

Figure 2. Same as figure 1, as for t $\bar{\text{t}}$ W^- production.

As the ordering variable in the POWHEG method is the relative transverse momentum, in case of an angular-ordered PS parton emissions with larger transverse momentum than the first one have to be vetoed explicitly (done in HERWIG automatically). Furthermore, a truncated shower, simulating wide-angle soft emission before the hardest one ought to be included, too. However, the effect of the truncated shower in general turns out to be small, as shown e.g. in ref. [23] and as we already verified in case of many different multiparticle production processes including a t $\bar{\text{t}}$ pair, where the predictions of PYTHIA and HERWIG turn out to agree one with each other within a few percent. Thus, we neglect truncated shower contributions in this paper, as we already did in our previous ones.

These SMC codes were also used to generate t-quark and heavy boson decays (neglecting spin correlations), as well as hadronization and hadron decays. For consistency, heavy particle masses in the SMC setup were set to the same values used in the PowHel computation, whereas the light quark masses in HERWIG were set to the default values implemented in PYTHIA. We allow for all decay modes of the t-quarks and vector bosons as implemented in the SMC's. Decays of heavy bosons into electrons were assumend to have the same branching ratio as into muons. π^0's were enforced to be stable in both SMC's, as they can be reconstructed in the experiments from their decay products (2 γ), and muon stability was enforced in HERWIG, as in PYTHIA default configuration. All other particles, taus and hadrons were assumed to be stable or to decay according to the default implementation of each SMC. Multiple interactions were neglected in both SMC's.

JHEP11(2012)056

3.2 Inclusive analysis

We now present predictions at the SMC level, i.e. after PS, hadronization and hadron decay, in case of $\mathrm{t}\,\bar{\mathrm{t}}\,W^+$, $\mathrm{t}\,\bar{\mathrm{t}}\,W^-$ and $\mathrm{t}\,\bar{\mathrm{t}}\,Z$ in the most general case, i.e. without applying any cut. This is possible since these processes are finite at the Born level, so we did not have to introduce any technical cut in the `PowHel` generation of LHE's. It is useful and instructive to present some theoretical distributions at this level, to better understand how the selection cuts that we will discuss in the following will modify these predictions. In particular, we focus on a few selected distributions that will also be shown again, in presence of cuts, in the following subsections.

The inclusive cross-sections at the SMC level are the same as at the NLO level as the POWHEG method ensures that the cross-sections from LHE's coincide with the exact NLO ones, i.e. $\sigma_{\mathrm{LHE}} = \sigma_{\mathrm{NLO}}$. We found that $\sigma_{\mathrm{t}\,\bar{\mathrm{t}}\,Z} > \sigma_{\mathrm{t}\,\bar{\mathrm{t}}\,W^+} > \sigma_{\mathrm{t}\,\bar{\mathrm{t}}\,W^-}$, with $\sigma_{\mathrm{t}\,\bar{\mathrm{t}}\,Z} = 137.21 \pm 0.01\,\mathrm{fb}$, $\sigma_{\mathrm{t}\,\bar{\mathrm{t}}\,W^+} = 106.74 \pm 0.01\,\mathrm{fb}$ and $\sigma_{\mathrm{t}\,\bar{\mathrm{t}}\,W^-} = 43.472 \pm 0.005\,\mathrm{fb}$, respectively (uncertainties are statistical only). These values are slightly larger than those quoted in table 1, due to the slightly smaller value of the t-quark mass (see the beginning of the previous subsection 3.1).

The invariant mass of all opposite-charge, same-flavour (ℓ^+, ℓ^-) pairs in all events is plotted in figure 3.a. Even in absence of cuts, a peak is well visible in the $\mathrm{t}\,\bar{\mathrm{t}}\,Z$ distribution, at m_Z, due to $Z \to \ell^+\ell^-$ decays. The presence of this peak, absent in the $\mathrm{t}\,\bar{\mathrm{t}}\,W^+$ and $\mathrm{t}\,\bar{\mathrm{t}}\,W^-$ distributions also plotted in figure 3.a, will be exploited in the trilepton analysis discussed in the following section 3.3. Looking at the invariant mass of all same-sign (anti-) lepton pairs (e^+e^+, $\mu^+\mu^+$, e^-e^-, $\mu^-\mu^-$, $e^+\mu^+$, $e^-\mu^-$) in all events, plotted in figure 3.b, an almost monotonically decreasing distribution is found, except for a small increase near zero. Near zero the behaviour in invariant-mass distribution is the opposite for the opposite-charge and same-charge lepton pairs. The small peak in the beginning of figure 3.a can be accounted mainly for electromagnetically decaying neutral mesons, that do not produce same-charge pairs.

The predictions using `HERWIG` as SMC, instead of `PYTHIA`, agree with the `PYTHIA` ones well below 5 % in all the dilepton mass range considered (see the ratios plotted in both lower panels of figure 3) when we switch off photon radiation from leptons in `PYTHIA`, which is default in `HERWIG`. Switching off photon radiation changes noticeably but the invariant mass of the same-flavour, opposite-charge leptons in figure 3.a in the range between 65 and 92 GeV, where the sharp peak seen by `HERWIG` is smeared in case of default `PYTHIA`.

In figure 4.a, the transverse momentum distribution of the hardest lepton of each event is shown. Here it is worth noting the different shapes of the $\mathrm{t}\,\bar{\mathrm{t}}\,W^+$ and $\mathrm{t}\,\bar{\mathrm{t}}\,W^-$ distributions, with the $\mathrm{t}\,\bar{\mathrm{t}}\,W^-$ becoming larger than the $\mathrm{t}\,\bar{\mathrm{t}}\,W^+$ one for $p_\perp > 270\,\mathrm{GeV}$, as expected because the high $p_\perp$ tail is populated by prompt leptons emitted from primary $W^- \to \ell\,\nu_\ell$ decays, that are absent in case of W^+ decays. Leptons originated by primary Z decays can have even larger $p_\perp$ as seen from the shape of the tail of the $\mathrm{t}\,\bar{\mathrm{t}}\,Z$ distribution, with a slope flatter than both the previous ones.

Finally, the missing transverse momentum distribution due to all neutrinos is plotted in figure 4.b. The shape of the $\mathrm{t}\,\bar{\mathrm{t}}\,W^+$ distribution is similar to the $\mathrm{t}\,\bar{\mathrm{t}}\,W^-$ one, with

JHEP11(2012)056

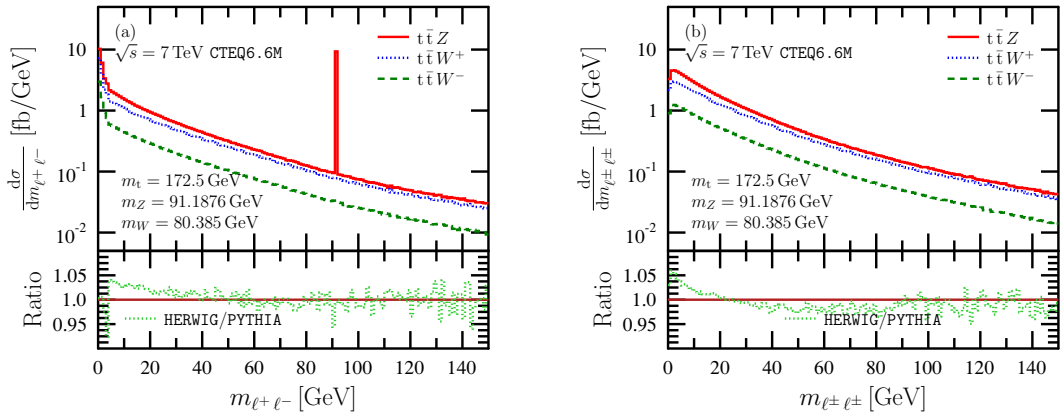

Figure 3. Invariant mass of a) all (ℓ^+, ℓ^-) same-flavour lepton-antilepton pairs and b) all (ℓ, ℓ) same-sign lepton and anti-lepton pairs from all events in the inclusive analysis, as obtained by PowHel + PYTHIA at the $\sqrt{s} = 7$ TeV LHC. Predictions for the three processes $t\bar{t}Z$, $t\bar{t}W^+$, and $t\bar{t}W^-$ are shown separately. In the lower panel, the ratio between the cumulative predictions of PowHel + HERWIG and PowHel + PYTHIA is also shown.

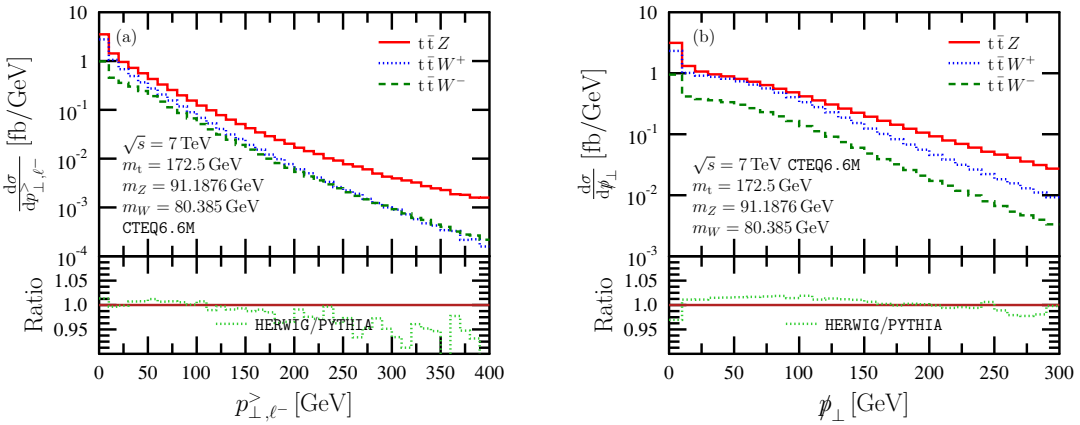

Figure 4. Distributions of a) the transverse momentum of the hardest lepton and b) the missing transverse momentum due to all neutrinos from all events in the no-cut analysis, as obtained by PowHel + PYTHIA at the $\sqrt{s} = 7$ TeV LHC. Predictions for the three processes $t\bar{t}Z$, $t\bar{t}W^+$, and $t\bar{t}W^-$ are shown separately. In the lower panel, the ratio between the cumulative predictions of PowHel + HERWIG and PowHel + PYTHIA is also shown.

a rescaling factor just due to the different cross-section, whereas the shape of the $t\bar{t}Z$ distributions differs from the previous ones, with a larger contribution in the first two bins, due to events without neutrinos or with neutrinos from secondary decays with very small transverse energy and a flatter slope than the $t\bar{t}W^{\pm}$ cases. The region around 50 GeV, where the the $t\bar{t}W^+$ and $t\bar{t}Z$ distributions are closer together, is filled by neutrinos from prompt W^+ decays, absent in case of $t\bar{t}Z$. The first bin is enhanced in all distributions due to the possibility of events without neutrinos (W decays in two light jets are indeed possible and not ruled out by any selection cut in this analysis).

JHEP11(2012)056

For both distributions plotted in figure 4 we found that the differences between the cumulative predictions by PYTHIA and HERWIG, obtained by summing over the three $t\bar{t}V$ processes, are within 5 % (see the lower panels), with a slightly larger agreement in case of the $\not{p}_\perp$-distribution.

3.3 Trilepton-channel analysis

The aim of the trilepton channel analysis proposed in ref. [2] is selecting $t\bar{t}Z$ events, with Z decaying in two opposite-sign charged leptons, and one of the quarks of the $t\bar{t}$-pair decaying leptonically, whereas the other one hadronically. In particular, we considered the following set of cuts:

1. at least two opposite-charge, same-flavor leptons with $p_{\perp,\ell} > 20\,\text{GeV}$ and within CMS acceptance ($|\eta_\ell| < 2.4$, with an additional cut on the electrons impinging on the barrel/endcap transition region of the electromagnetic calorimeter (ECAL), corresponding to the pseudorapidity interval $1.4442 < |\eta_\ell| < 1.566$),
2. constrain the invariant mass of the dilepton system ("reconstructed Z") within the $81\,\text{GeV} < m_{\ell\ell} < 101\,\text{GeV}$ interval,
3. $p_{\perp,\ell\ell} > 35\,\text{GeV}$, where $p_{\perp,\ell\ell}$ is the transverse momentum of the reconstructed Z,
4. at least a third lepton in the event with $p_{\perp,\ell_3} > 10\,\text{GeV}$ and obeying the same pseudorapidity requirements as the other two leptons,
5. at least three jets with $p_{\perp,j} > 20\,\text{GeV}$ and $|\eta_j| < 2.4$, of which two positively b-tagged,
6. $H_\text{T} > 120\,\text{GeV}$, defined as the scalar sum of the transverse momenta of all jets with $p_{\perp,j} > 20\,\text{GeV}$ and $|\eta_j| < 2.4$.

In our simulation, jets were reconstructed using the anti-$k_\perp$ algorithm [24], with $R = 0.5$, using `Fastjet 3.0.0` [25]. b-tagging was done by means of the MCTRUTH parameter, allowing to trace back the origin of a jet to a b or a $\bar{\text{b}}$ quark. In case of multiple dilepton pairs with opposite charge and same flavour satisfying cuts 1), 2) and 3), the pair with the invariant mass closest to the nominal Z mass was selected.

Predictions for the expected number of events after cuts at the $\sqrt{s} = 7\,\text{TeV}$ LHC, corresponding to an integrated luminosity $L = 4.98\,\text{fb}^{-1}$, as obtained by our PowHel+PYTHIA simulations, are shown in figure 5, distinguishing the possible decay channels, labelled by the flavours of the two leptons entering the dilepton system plus the third lepton mentioned in cut 4). When more than one additional lepton satisfies cut 4), we choose that with the largest $p_\perp$. The sum of the results in all channels is plotted in the last bin of the figure, as well. These predictions can be compared to the experimental results, presented in ref. [2] for the same luminosity, with the caveat that we still do not include the predictions for background processes (like Z + jets, $t\bar{t}$ and diboson production) at the same accuracy. For an estimate of these background contributions at a lower accuracy, one can rely on ref. [2]. One has also to take into account that the CMS Collaboration used an experimental b-jet tagging algorithm, instead of a purely theoretical one, as we did.

JHEP11(2012)056

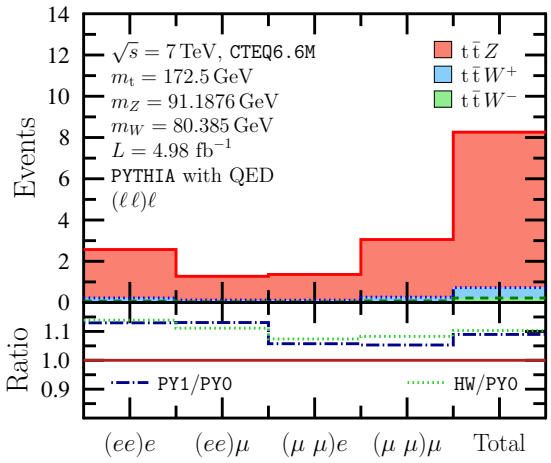

Figure 5. Number of events in the trilepton channels at the $\sqrt{s} = 7\,\text{TeV}$ LHC, as predicted by PowHel + PYTHIA, for an integrated luminosity amounting to $L = 4.98\,\text{fb}^{-1}$. The contribution in the $(e,\, e)\, e$, $(e,\, e)\, \mu$, $(\mu,\, \mu)\, e$ and $(\mu,\, \mu)\, \mu$ channels are shown separately, as well as their sum in the last bin. The contributions due to t $\bar{\text{t}}$ Z, t $\bar{\text{t}}$ W^+ and t $\bar{\text{t}}$ W^- are cumulated one over the other. To be compared with the experimental data in figure 4 of the CMS technical report [2]. In the lower inset the ratios between cumulative results using different SMC (HERWIG/PYTHIA) and between cumulative results obtained by neglecting and including photon radiation from leptons (PY1/PY0) are shown.

As expected, as a result of the selection cuts, and in particular of the cut on the invariant mass of the dilepton system, both in the experiment and in our theoretical predictions the contributions to the total number of events due to the t $\bar{\text{t}}$ $W^{\pm}$ processes are highly suppressed. We estimate a suppression factor of about 10 between the cross-sections after the cuts for the processes (t $\bar{\text{t}}$ W^++ t $\bar{\text{t}}$ W^-) and t $\bar{\text{t}}$ Z, from our theoretical simulations. The invariant mass of the reconstructed Z is plotted for these three processes in figure 6.a, from where it is clear that the largest contribution of the t $\bar{\text{t}}$ Z process is due to the peak around m_Z, completely absent in case of both t $\bar{\text{t}}$ W^+ and t $\bar{\text{t}}$ W^-.

In the lower inset of figure 5 the ratios of the results using different SMC's are plotted. In particular, using HERWIG instead of PYTHIA as SMC, leads to a larger number of events. This is due to the different physics implemented in the two SMC's. In fact, as already mentioned in section 3.2, while PYTHIA includes by default photon radiation from leptons, the stand-alone fortran version of HERWIG does not include it (unless one interfaces it with external packages). The photon radiation effect affects the dilepton invariant mass after SMC: as shown in figure 6.b, the very narrow peak evident in case of HERWIG simulations is smeared by the effect of photon radiation from leptons implemented in default PYTHIA simulations. As a further check, we switched off this kind of emissions even in PYTHIA. The predictions of PYTHIA without lepton radiation are superimposed on the same plot and look to be closer to the HERWIG ones. The modification on the number of events after cuts in the different channels, one gets by switching off this effect in PYTHIA, is also shown in the lower panel of figure 5.

JHEP11(2012)056

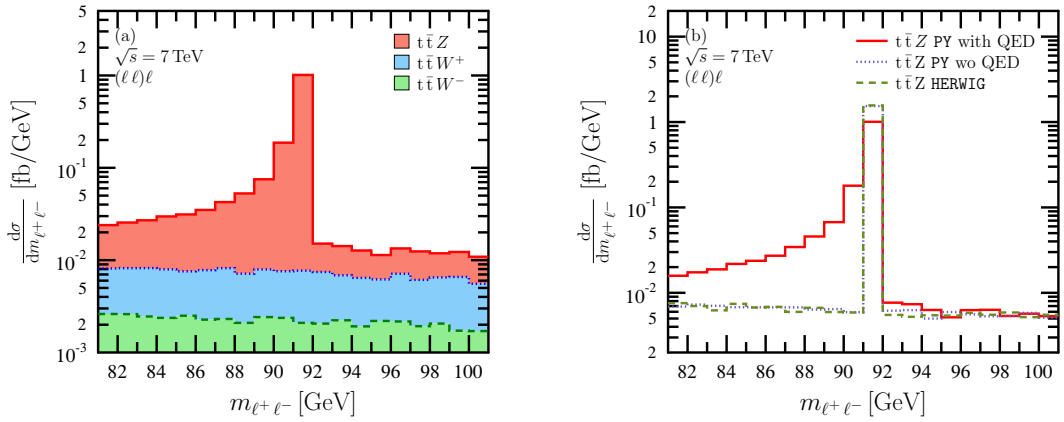

Figure 6. Invariant mass of the Z reconstructed from same-flavour (ℓ^+, ℓ^-) pairs after the trilepton analysis, as obtained by `PowHel+ PYTHIA` at the $\sqrt{s} = 7$ TeV LHC. a) Predictions corresponding to the different processes t $\bar{\text{t}}$ Z, t $\bar{\text{t}}$ W^+ and t $\bar{\text{t}}$ W^- cumulated one over the other, b) distributions obtained by using different SMC (`PYTHIA`, `HERWIG` and `PYTHIA` without photon radiation from leptons) are shown, limited to t $\bar{\text{t}}$ Z-production.

The predictions presented in figure 5 are compatible with the experimental data of ref. [2] within the error-bars of the latter. However, while our simulations predict almost symmetric central values between the (e, e) e and the (μ, μ) μ channels, and between the (e, e) μ and the (μ, μ) e channels, the experimental data show the same pattern for the latter case, but different for the first one: the (μ, μ) μ bin is more populated than the (e, e) e one (although the populations of these two bins can still be viewed equal within the large error-bars). From our simulations we verified that a slight asymmetry between the (e, e) e and the (μ, μ) μ bins is generated by the inclusion of photon radiation from leptons. In the absence of this effect, the population of these two channels is instead completely symmetric. It is also affected by the different selection cuts on electrons and muons (see cut 1). We think that the larger asymmetry effects, as inferred from the experimental data, are due to other experimental details, like limited detection efficiencies and charge misidentification effects. Such effects are neglected in our simulations and their precise implementation is dependent on the experimental analysis detail, beyond the scope of this work.

Our predictions for the cross-section contributions in the different trilepton channels (see figure 5), summing over the three processes t $\bar{\text{t}}$ Z, t $\bar{\text{t}}$ W^+ and t $\bar{\text{t}}$ W^-, in case of $\sqrt{s} = 7$ TeV LHC, are as follows: $\sigma_{(e,e),e} = 0.516$ fb, $\sigma_{(e,e),\mu} = 0.255$ fb, $\sigma_{(\mu,\mu),e} = 0.273$ fb, $\sigma_{(\mu,\mu),\mu} = 0.613$ fb, $\sigma_{\sum} = 1.658$ fb, all with a statistical uncertainty smaller than one unit change in the last significant digit.

The transverse momentum distributions of the leading and subleading (anti-)lepton of the (ℓ^+, ℓ^-) pairs selected by the considered system of cuts are shown separately in figure 7. These distributions have different shapes, as expected: those belonging to the leading lepton are peaked at ~ 65 GeV for both t $\bar{\text{t}}$ Z, t $\bar{\text{t}}$ W^+ and t $\bar{\text{t}}$ W^- while those belonging to the subleding lepton decrease monotonically just above the $p_{\perp,l} > 20$ GeV cut. When considered together, the lepton and the anti-lepton give rise to a "reconstructed Z", whose $p_\perp$ has a shape characterized by a smooth peak in the 50 GeV region.

JHEP11(2012)056

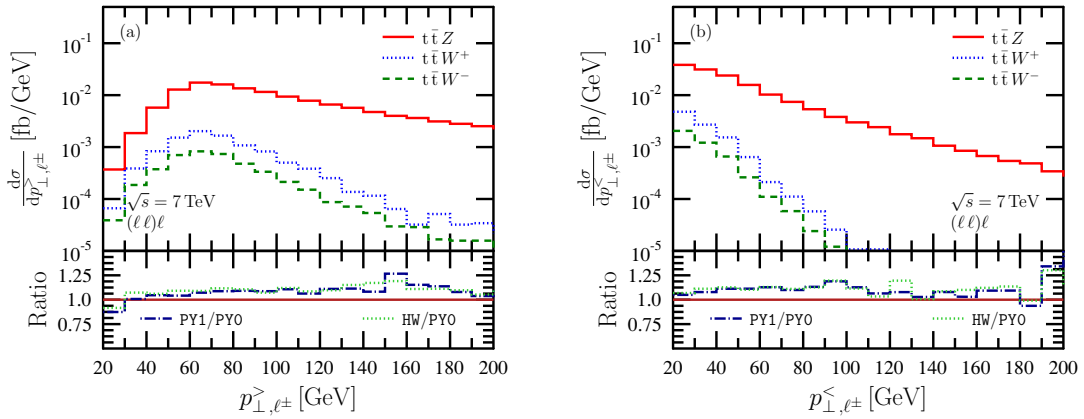

Figure 7. Transverse momentum distributions of a) the leading and b) the subleading (anti-)lepton of each (ℓ^+, ℓ^-) pair corresponding to a reconstructed Z boson. Predictions by `PowHel` + `PYTHIA`, corresponding to the different t $\bar{\text{t}}$ Z, t $\bar{\text{t}}$ $W^+$and t $\bar{\text{t}}$ W^- processes are shown separately. In the lower inset the ratios between cumulative results using different SMC `HERWIG` and `PYTHIA` (`HW/PY0`) and between cumulative results obtained by neglecting and including photon radiation from leptons in `PYTHIA` (`PY1/PY0`) are shown.

It is also interesting to separate the behaviour of leptons and anti-leptons. As seen in figure 8.a, the $p_\perp$-distribution of the hardest lepton of each event has a plateau in the region 20-70 GeV in case of both t $\bar{\text{t}}$ Z and t $\bar{\text{t}}$ W^+, whereas for the distribution of the hardest anti-lepton plotted in figure 8.b, the plateau appears for t $\bar{\text{t}}$ Z and t $\bar{\text{t}}$ W^-, i.e. the situation for t $\bar{\text{t}}$ W^+ and t $\bar{\text{t}}$ W^- is symmetric. This symmetry suggests that these plateaus are generated by the selection cuts and include the contributions of the prompt leptons and anti-leptons originated directly from the decay of the initial Z and W weak-bosons (whereas possible secondary leptons or anti-leptons with the same transverse momentum are cut). The behaviour of the tails of the t $\bar{\text{t}}$ W^+ and t $\bar{\text{t}}$ W^- distributions in figure 8.b is the same as already observed in figure 4.a for the case of the inclusive analysis (see discussion in subsection 3.2), suggesting that even the high-$p_\perp$ regions are dominated by prompt leptons, as expected. In case of both `HERWIG` and `PYTHIA` where the photon radiation effect is switched off, these distributions are just increased by 5-10 %.

We also repeated the analysis in the trilepton channel in case of an LHC $\sqrt{s} = 8$ TeV center-of-mass energy, that can be useful in view of future data analysis on the basis of the events recorded in the present run. For future reference, we report here our cumulative predictions for the cross-section contributions of the three processes t $\bar{\text{t}}$ Z, t $\bar{\text{t}}$ W^+ and t $\bar{\text{t}}$ W^- at $\sqrt{s} = 8$ TeV: $\sigma_{(e,e),e} = 0.782$ fb, $\sigma_{(e,e),\mu} = 0.388$ fb, $\sigma_{(\mu,\mu),e} = 0.420$ fb, $\sigma_{(\mu,\mu),\mu} = 0.934$ fb, $\sigma_\Sigma = 2.524$ fb, all with a statistical uncertainty smaller than one unit change in the last significant digit. Furthermore, predictions for the same differential distributions already discussed in the $\sqrt{s} = 7$ TeV case, were produced in the 8 TeV case, and we have found very similar results, except for a rescaling factor just given by the ratio of the cross-sections at 8 and 7 TeV. The LHE's are freely available at our web repository: `http://www.grid.kfki.hu/twiki/bin/view/DbTheory/WebHome`.

JHEP11(2012)056

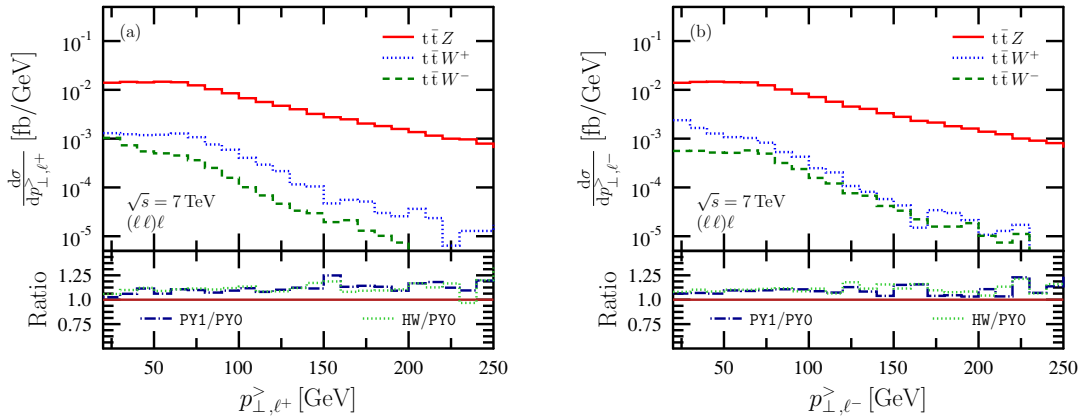

Figure 8. Transverse momentum distributions of a) the hardest anti-lepton and b) the hardest lepton of each event, at $\sqrt{s} = 7\,\text{TeV}$ LHC, as predicted by `PowHel` + `PYTHIA` after the trilepton analysis for the processes $t\,\bar{t}\,Z$ (solid), $t\,\bar{t}\,W^+$ (dotted) and $t\,\bar{t}\,W^-$ (dashed). In the lower inset the ratios between cumulative results using different SMC `HERWIG` and `PYTHIA` (`HW/PY0`) and between cumulative results obtained by neglecting and including photon radiation from leptons in `PYTHIA` (`PY1/PY0`) are shown.

3.4 Dilepton-channel analysis

As mentioned in the introduction, studies of $t\,\bar{t}\,V$ decays in the dilepton channel, with two same-sign leptons plus jets, have their original motivation that this kind of signature is hardly produced by SM processes, and can thus be used in searches for supersymmetry. In this case, $t\,\bar{t}\,V$ can be considered as a background with respect to possible new physics processes. Other sizable backgrounds involve many different diboson and triboson production processes. An exhaustive list of backgrounds in this context can be found in ref. [13]. New physics searches usually also involve a cut on missing energy. In this paper we explore the dilepton channel, without imposing any missing energy cut, as also done in the very recent CMS technical report [2], where the analysis was optimized on the basis of data collected at LHC at $\sqrt{s} = 7\,\text{TeV}$ corresponding to an integrated luminosity $L = 4.98\,\text{fb}^{-1}$. This way the relatively small number of $t\,\bar{t}\,V$ events does not suffer any further suppression due to this cut.

The aim of this analysis is to select the events where one of the quarks of the $t\,\bar{t}$-pair decays leptonically and the other one hadronically, and the vector boson decays leptonically giving rise to a lepton with the same sign of the lepton coming from the (anti-)quark. In case of $t\,\bar{t}\,W^+$-production this means that we are looking for $W^+ \to \ell^+\,\nu_\ell$, accompanied by the leptonic decay of the t-quark, whereas, in case of $t\,\bar{t}\,W^-$-production we aim to select events with $W^- \to \ell^-\,\bar{\nu}_\ell$, accompanied by the leptonic decay of the $\bar{t}$-quark. In case of $t\,\bar{t}\,Z$-production $Z \to \ell^+\ell^-$, and thus it is sufficient that either the t- or the $\bar{t}$-quark decays leptonically.

Following the CMS Collaboration, we considered the following set of cuts:

1. two same-sign isolated leptons with $p_{\perp,\ell_1} > 55\,\text{GeV}$ and $p_{\perp,\ell_2} > 30\,\text{GeV}$, respectively, within CMS acceptance ($|\eta_\ell| < 2.4$, plus a further removal of the [1.4442, 1.566]

JHEP11(2012)056

pseudorapidity range corresponding to the ECAL barrel/endcap transition region, applied in case of electrons),

2. dilepton invariant mass $m_{\ell_1,\ell_2} > 8\,\text{GeV}$,

3. at least 3 jets with $p_{\perp,j} > 20\,\text{GeV}$ and $|\eta_j| < 2.4$, satisfying the additional cut $\Delta R(j,\ell) > 0.4$ on the distance in the pseudorapidity-azimuthal angle plane, for both $\ell = \ell_1, \ell_2$,

4. at least one of the previous 3 jets must be b-tagged,

5. $H_\text{T} > 100\,\text{GeV}$, where H_T is computed as the scalar sum of the transverse momenta of all jets satisfying cut 3).

Jets were constructed using of the anti-k$_\perp$ algorithm [24], with $R = 0.5$, as implemented in `Fastjet 3.0.0` [25]. Lepton isolation was computed by making use of the standard isolation criterion mentioned in the CMS technical report [1]: we require a lepton relative isolation $I_\text{rel} > 0.15$, where I_rel is computed as the ratio between the scalar sum of the transverse momenta of all tracks within a distance $\Delta R < 0.3$ with respect to the selected lepton and the transverse momentum of the lepton itself (excluded from the sum at the numerator). Furthermore, in case of multiple dilepton pairs satisfying the cuts mentioned above, the pair was selected with the largest combined transverse momentum.

As also done in the CMS analysis [2], we explicitly exclude from this analysis all events that are selected in the trilepton channel analysis, in order to obtain two statistically independent samples (trilepton veto). As we will see in the following, the final predictions in the dilepton channel as for both the number of events and the shape of the distributions, will indeed be affected by this choice, especially as for the $\text{t}\,\bar{\text{t}}\,Z$ process.

Differences between our theoretical analysis framework and the experimental conditions are listed in the following:

- Contrary to experimental reconstruction of the events, electron and muon detection efficiencies in our theoretical simulations were assumed to be 100 % and charge misidentification effects neglected.

- Also, while in the experiment b-jets were reconstructed as displaced vertices, making use of spatial tracking information, and a b-tagging algorithm was applied, ensuring a limited efficiency in the reconstruction of b-jets, accompanied by a non-negligible fake rate, in our simulations we identified b-jets using the `MCTRUTH` parameter which allows for tracking back b and $\bar{\text{b}}$ quarks from $\text{t}\,\bar{\text{t}}$-decay, but we lacked spatial information concerning the position of displaced vertices.

Despite the differences in the analysis, and perhaps other experimental detail we are not aware of, the theoretical predictions, shown in figure 9, are compatible with the experimental results.

The largest contribution to the total number of events is from the $\text{t}\,\bar{\text{t}}\,W^+$ process, followed by the $\text{t}\,\bar{\text{t}}\,Z$ and the $\text{t}\,\bar{\text{t}}\,W^-$ ones. The contribution of the $\text{t}\,\bar{\text{t}}\,W^+$ process is

JHEP11(2012)056

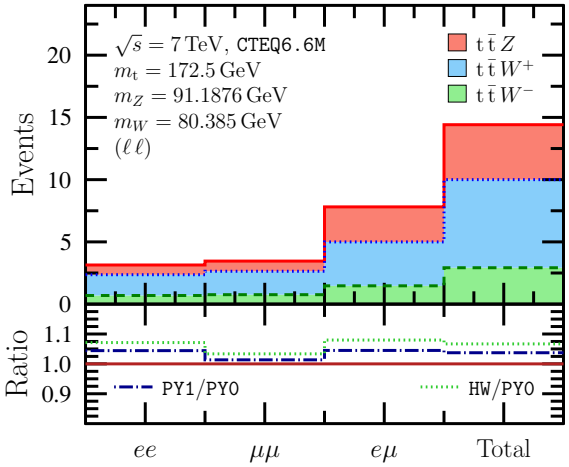

Figure 9. Number of events in the dilepton channel at $\sqrt{s} = 7$ TeV LHC, as predicted by PowHel + PYTHIA, for an integrated luminosity $L = 4.98\,\text{fb}^{-1}$. The contribution in the (e, e), (μ, μ), (e, μ) channels are shown separately, as well as their sum in the last bin. The contributions due to $t\,\bar{t}\,Z$, $t\,\bar{t}\,W^+$ and $t\,\bar{t}\,W^-$ are cumulated one over the other. In the lower inset the ratios between cumulative results using different SMC HERWIG and PYTHIA (HW/PY0) and between cumulative results obtained by neglecting and including photon radiation from leptons in PYTHIA (PY1/PY0) are shown.

larger than the $t\,\bar{t}\,W^-$ one already at the inclusive level (see section 3.3), with the ratio between the two remaining almost the same after cuts (2.45 for the inclusive predictions and 2.42 after cuts). The contribution of $t\,\bar{t}\,W^+$ is enhanced with respect to that of $t\,\bar{t}\,Z$ after cuts due to the effect of the selection cuts and of the trilepton veto. For the $t\,\bar{t}\,W^\pm$ processes, the contribution in the (e, μ) channel turns out to be almost twice the average of the (e, e) and (μ, μ) ones, as naively expected on the basis of the possible charge and flavour combinations. (An electron can come from the W and a muon with the same sign from one of the t-quarks, or viceversa.) For the $t\,\bar{t}\,Z$ process, the contribution in the (e, μ) channel turns out to be $\simeq 3.5$ times the average of the (e, e) and (μ, μ) ones, i.e. larger than expected on the basis of the charge and flavour combinatorics. The reason has to be attributed to the trilepton veto. As seen in figure 5, the number of events in the trilepton channel in case of the (e, e) e and (μ, μ) μ combinations are larger than those in the (e, e) μ and (μ, μ) e bins. The former affect the (e, e) and (μ, μ) bins of the dilepton analysis, while the latter affect the (e, μ) bins of the dilepton analysis. As a consequence, the contribution to the (e, μ) channel of the dilepton analysis is less suppressed than those in the (e, e) and (μ, μ) channels due to the trilepton veto. The predictions by different SMC programs, i.e. HERWIG and PYTHIA where the photon radiation from leptons is switched off, are up to 8 % and 5 % larger than those of PYTHIA, as can be seen from the lower panel of figure 9. These differences have the same sign, but are smaller, than those found in case of the trilepton analysis (see the lower panel of figure 5 for comparison).

The PowHel + PYTHIA predictions for the cross-section contributions in the different dilepton channels (see figure 9), summing over $t\,\bar{t}\,Z$, $t\,\bar{t}\,W^+$ and $t\,\bar{t}\,W^-$, in case of

JHEP11(2012)056

$\sqrt{s} = 7\,\text{TeV}$ LHC are listed in the following, together with their sum: $\sigma_{(e,e)} = 0.631\,\text{fb}$, $\sigma_{(e,\mu)} = 0.694\,\text{fb}$, $\sigma_{(\mu,\mu)} = 1.569\,\text{fb}$, $\sigma_{\sum} = 2.894\,\text{fb}$, all with a statistical uncertainty smaller than one unit change in the last significant digit.

As for the comparison with the experimental data, we note that in the CMS technical report [2] a contribution to the number of events was assigned to the effect of charge misidentification for the leptons, in particular the electrons, and another additional contribution to the effect of non-prompt leptons, i.e. leptons not coming directly from heavy bosons decays. In our theoretical simulations the background due to charge misidentification vanishes, whereas a possible contribution of non-prompt leptons to our final results relies on the effectiveness of the isolation criteria we adopted. In this respect, even if we lack a precise estimate, it can be interesting to observe the differential distributions of the hardest isolated (anti-)leptons of each event after cuts, plotted in figure 10.

We see from figure 10.a, in case of $\mathrm{t}\,\bar{\mathrm{t}}\,W^+$ the hardest isolated anti-lepton after cuts has a minimum $p_\perp$ of 50 GeV and a peak slightly above it, whereas in case of $\mathrm{t}\,\bar{\mathrm{t}}\,W^-$ it has a minimum $p_\perp$ of 30 GeV without a peak. In case of the hardest isolated lepton, instead, the behaviour of $\mathrm{t}\,\bar{\mathrm{t}}\,W^+$ and $\mathrm{t}\,\bar{\mathrm{t}}\,W^-$ is the opposite, as can be seen in figure 10.b. This behaviour is compatible with cut 1) and means that the system of proposed cuts is effective in selecting prompt leptons, i.e. the selection of $(\ell^+,\,\ell^+)$ pair in case of $\mathrm{t}\,\bar{\mathrm{t}}\,W^-$ decay, or of $(\ell^-,\,\ell^-)$ pair in the $\mathrm{t}\,\bar{\mathrm{t}}\,W^+$ decay are actually suppressed by orders of magnitude, even if several leptons and anti-leptons can be present after PS, hadronization and hadron decays. In case of $\mathrm{t}\,\bar{\mathrm{t}}\,Z$ decays, two opposite-charge leptons are produced by Z-decays, so both $(\ell^+,\,\ell^+)$ and $(\ell^-,\,\ell^-)$ pairs of prompt leptons could be selected. Thus a peak above 50 GeV is present in both the lepton and the anti-lepton distributions. In all cases, the peaks slightly above 50 GeV are related to the request of having at least one (anti-)lepton with $p_\perp > 55\,\text{GeV}$ in the selection cuts.

As examples of further distributions that can be measured in the experiment, the cumulative transverse momentum distributions of the leading and subleading lepton or anti-lepton of the $(\ell,\,\ell)$ selected pairs are plotted in figure 11. At low $p_\perp$ the sum is dominated by the $\mathrm{t}\,\bar{\mathrm{t}}\,W^+$ contribution, whereas in the high $p_\perp$ tail (i.e. above $\simeq 300\,\text{GeV}$ in case of the leading lepton and above $\simeq 150\,\text{GeV}$ in case of the subleading one), the contributions of $\mathrm{t}\,\bar{\mathrm{t}}\,Z$ and $\mathrm{t}\,\bar{\mathrm{t}}\,W^+$ become almost equal.

In view of the searches for new physics in the dilepton channel, another interesting distribution is that of the missing transverse energy, plotted in figure 12. In figure 12.a, different shapes characterize the three $\mathrm{t}\,\bar{\mathrm{t}}\,V$ processes. The distribution for $\mathrm{t}\,\bar{\mathrm{t}}\,Z$ is peaked around 30 GeV, while that for $\mathrm{t}\,\bar{\mathrm{t}}\,W^\pm$ is peaked around 50 GeV. This difference is related to the $W \to \ell\,\nu_\ell$ decay events selected in the dilepton analysis, that populate the peak region. The suppression in the first few bins, not present in the analogous inclusive $\not{p}_\perp$-distribution plotted in figure 4.b, is an effect of the set of cuts, aiming at the selection of two same-sign prompt (anti-)leptons. With this selection both the primary boson and either the t- or the $\bar{t}$-quark should decay leptonically, leading to a non-zero $\not{p}_\perp$. As expected, including further cuts on $\not{p}_\perp$, will enhance the relative contribution of the $\mathrm{t}\,\bar{\mathrm{t}}\,W^\pm$ process with respect to the $\mathrm{t}\,\bar{\mathrm{t}}\,Z$ one, and will reduce the number of observed $\mathrm{t}\,\bar{\mathrm{t}}\,V$ events. In particular, integrating over the cumulative $\not{p}_\perp$-distribution, plotted in figure 12.b, we find

JHEP11(2012)056

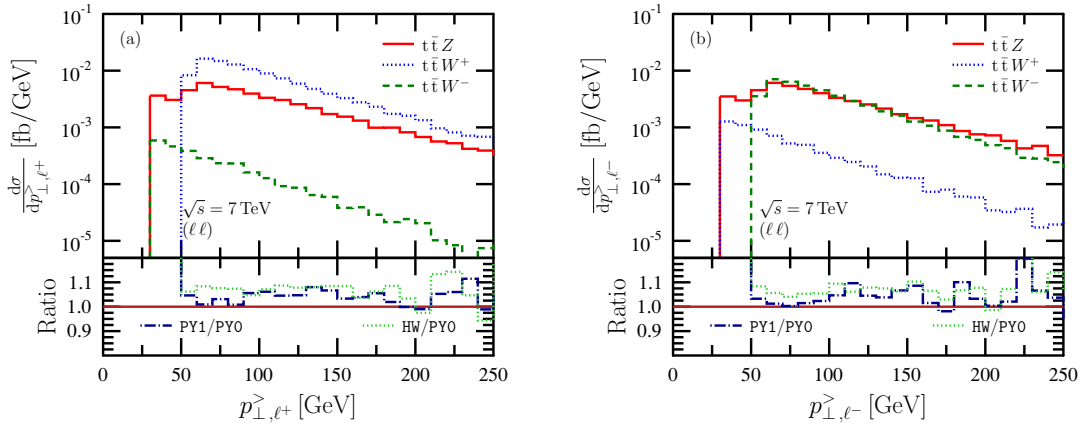

Figure 10. Transverse momentum distributions of a) the hardest anti-lepton and b) the hardest lepton of each event at $\sqrt{s} = 7\,\text{TeV}$ LHC, as predicted by `PowHel` + `PYTHIA` after the dilepton analysis. The distributions for $t\,\bar{t}\,Z$, $t\,\bar{t}\,W^+$ and $t\,\bar{t}\,W^-$ are shown by solid (red), dotted (blue) and dashed (green) lines, respectively. In the lower inset the ratios between cumulative results using different SMC `HERWIG` and `PYTHIA` (`HW/PY0`) and between cumulative results obtained by neglecting and including photon radiation from leptons in `PYTHIA` (`PY1/PY0`) are shown.

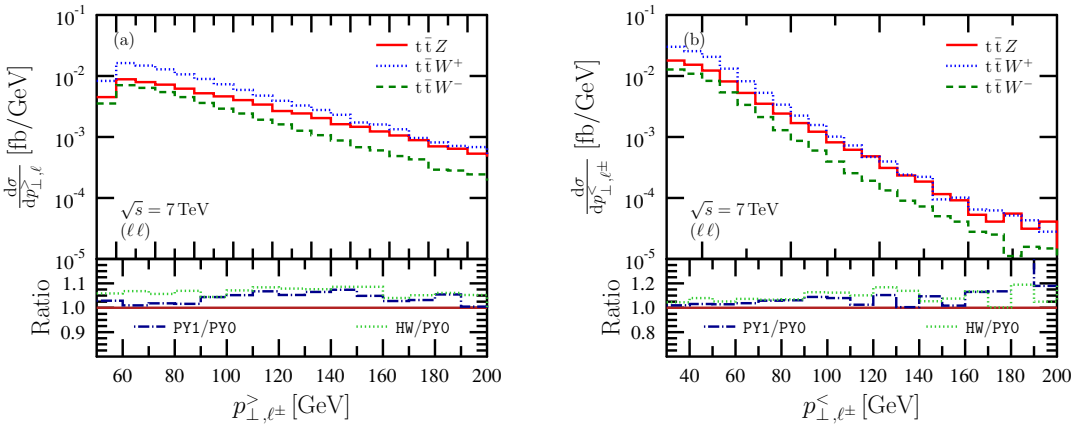

Figure 11. Transverse momentum distribution of a) the leading and b) the subleading (anti)-lepton of each same-sign (ℓ, ℓ) pair after the dilepton analysis. Predictions by `PowHel` + `PYTHIA` at $\sqrt{s} = 7\,\text{TeV}$ LHC corresponding to the different $t\,\bar{t}\,Z$, $t\,\bar{t}\,W^+$and $t\,\bar{t}\,W^-$ processes are shown separately. In the lower inset the ratios between cumulative results using different SMC `HERWIG` and `PYTHIA` (`HW/PY0`) and between cumulative results obtained by neglecting and including photon radiation from leptons in `PYTHIA` (`PY1/PY0`) are shown.

that a cut of $\not{p}_\perp > 50\,\text{GeV}$ corresponds to a reduction on the total number of events, plotted in figure 9, by a factor of $\simeq 4$ and a cut of $\not{p}_\perp > 100\,\text{GeV}$ to a further reduction by a similar factor.

Looking forward to an analysis of data collected in the recent LHC energy upgrade, we repeated the whole analysis at $\sqrt{s} = 8\,\text{TeV}$ LHC. For future reference, we list our predictions for the cross-sections after cuts at this energy for each dilepton channel, together with their sum. We found $\sigma_{(e,e)} = 0.907\,\text{fb}$, $\sigma_{(e,\mu)} = 0.991\,\text{fb}$, $\sigma_{(\mu,\mu)} = 2.289\,\text{fb}$, $\sigma_\Sigma = 4.187\,\text{fb}$,

JHEP11(2012)056

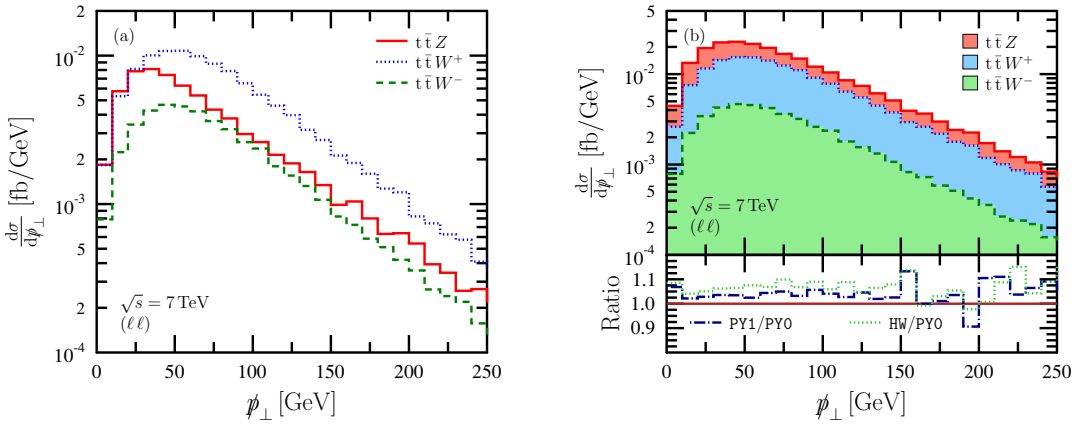

Figure 12. Missing transverse momentum distribution at $\sqrt{s} = 7$ TeV LHC, as predicted by PowHel + PYTHIA after the dilepton analysis. a) distributions for the processes t $\bar{\text{t}}$ Z (solid), t $\bar{\text{t}}$ W^+ (dotted) and t $\bar{\text{t}}$ W^- (dashed) lines. b) these different contributions are added one over the other in a cumulative way. In the lower inset the ratios between cumulative results using different SMC HERWIG and PYTHIA (HW/PY0) and between cumulative results obtained by neglecting and including photon radiation from leptons in PYTHIA (PY1/PY0) are shown.

all with a statistical uncertainty smaller than one unit change in the last significant digit. As for differential distributions at 8 TeV, we found that their general qualitative behaviour and their shapes are similar to those already shown at 7 TeV, thus we do not present them again here. These can just be obtained by a proper rescaling factor given by the ratio of the cross-sections at 8 and 7 TeV. The LHE's are freely available at our web repository.

4 Conclusions

In this paper we provided predictions for t $\bar{\text{t}}$ V hadroproduction at LHC. Our NLO predictions in the t $\bar{\text{t}}$ $W^{\pm}$ channel provide a confirmation, by a completely independent method, of those already presented by ref. [13] at 7, 8 and 14 TeV center-of-mass energies. In case of both t $\bar{\text{t}}$ Z and t $\bar{\text{t}}$ $W^{\pm}$ we quote the uncertainties on the cross-sections due to scale variation at NLO. Furthermore, we provide predictions for differential distributions due to these same processes at the hadron level, thanks to the matching of the NLO computation with a SMC approach, through the POWHEG method as implemented in the PowHel framework, on the basis of the interface of the POWHEG-BOX and the HELAC-NLO event generators. In case of t $\bar{\text{t}}$ $W^{\pm}$ these are the first predictions provided at such a level of accuracy in the literature, whereas in case of t $\bar{\text{t}}$ Z this paper can be considered a sequel to our previous ones, exploring different decay channels in the phenomenological analysis. In particular, we concentrate on the dilepton and trilepton channels, also recently studied by the CMS Collaboration.

At 7 TeV our predictions turn out to be compatible with the experimental data, taking into account the slightly different selection conditions, whereas, in case of 8 TeV, where the experimental data have not yet been analyzed, we provide new predictions that we hope can be useful for the experimental analysis. For this purpose all LHE files with sets of several

JHEP11(2012)056

millions of events at the first radiation emission level used for the analysis presented in this paper, are freely available at our web repository: `http://www.grid.kfki.hu/twiki/bin/view/DbTheory/WebHome`.

In the future, when the accumulated data will reach the necessary statistics that allows for a more detailed comparison of the theory with the experiment, the inclusion of spin correlation effects and radiative corrections in top quark and heavy bosons decays, as well as the evaluation of the different backgrounds at the same level of accuracy, will be possible and indispensable. Moreover the estimate of the theoretical uncertainty will require further studies of the scale variation at the NLO and SMC levels, as well as a systematic study of the effect of different PDF sets and parameters.

Acknowledgments

This research was supported by the LHCPhenoNet network PITN-GA-2010-264564, the Swiss National Science Foundation Joint Research Project SCOPES IZ73Z0_1/28079, the TÁMOP 4.2.1./B-09/1/KONV-2010-0007 and 4.2.2/B-10/1-2010-0024 projects, the Hungarian Scientific Research Fund grant K-101482 and the Slovenian Ministery of Work under the Ad-Futura program. We are grateful to G. Dissertori, F. Pandolfi and P. Skands for useful discussions.

References

[1] CMS collaboration, S. Chatrchyan et al., *Search for new physics with same-sign isolated dilepton events with jets and missing transverse energy*, *Phys. Rev. Lett.* **109** (2012) 071803 [arXiv:1205.6615] [INSPIRE].

[2] CMS collaboration, *Measurement of the associated production of vector bosons with top-antitop pairs at 7 TeV*, PAS-TOP-12-014 (2012).

[3] S. Alioli, P. Nason, C. Oleari and E. Re, *A general framework for implementing NLO calculations in shower Monte Carlo programs: the POWHEG BOX*, *JHEP* **06** (2010) 043 [arXiv:1002.2581] [INSPIRE].

[4] S. Frixione, P. Nason and C. Oleari, *Matching NLO QCD computations with parton shower simulations: the POWHEG method*, *JHEP* **11** (2007) 070 [arXiv:0709.2092] [INSPIRE].

[5] P. Nason, *A new method for combining NLO QCD with shower Monte Carlo algorithms*, *JHEP* **11** (2004) 040 [hep-ph/0409146] [INSPIRE].

[6] G. Bevilacqua, M. Czakon, M. Garzelli, A. van Hameren, A. Kardos, et al., *HELAC-NLO*, arXiv:1110.1499 [INSPIRE].

[7] A. Kardos, C. Papadopoulos and Z. Trócsányi, *Top quark pair production in association with a jet with NLO parton showering*, *Phys. Lett.* **B 705** (2011) 76 [arXiv:1101.2672] [INSPIRE].

JHEP11(2012)056

[8] M. Garzelli, A. Kardos, C. Papadopoulos and Z. Trócsányi, *Standard model Higgs boson production in association with a top anti-top pair at NLO with parton showering*, *Europhys. Lett.* **96** (2011) 11001 [arXiv:1108.0387] [INSPIRE].

[9] M. Garzelli, A. Kardos and Z. Trócsányi, *NLO event samples for the LHC*, *PoS* **EPS-HEP2011** (2011) 282 [arXiv:1111.1446] [INSPIRE].

[10] S. Dittmaier, S. Dittmaier, C. Mariotti, G. Passarino, R. Tanaka, et al., *Handbook of LHC Higgs cross sections: 2. Differential distributions*, arXiv:1201.3084 [INSPIRE].

[11] A. Kardos, Z. Trócsányi and C. Papadopoulos, *Top quark pair production in association with a Z-boson at NLO accuracy*, *Phys. Rev.* **D 85** (2012) 054015 [arXiv:1111.0610] [INSPIRE].

[12] M. Garzelli, A. Kardos, C. Papadopoulos and Z. Trócsányi, *Z0 - Boson production in association with a top anti-top pair at NLO accuracy with parton shower effects*, *Phys. Rev.* **D 85** (2012) 074022 [arXiv:1111.1444] [INSPIRE].

[13] J.M. Campbell and R.K. Ellis, $t\bar{t}W^{\pm}$ *production and decay at NLO*, *JHEP* **07** (2012) 052 [arXiv:1204.5678] [INSPIRE].

[14] T. Sjöstrand, S. Mrenna and P.Z. Skands, *PYTHIA 6.4 physics and manual*, *JHEP* **05** (2006) 026 [hep-ph/0603175] [INSPIRE].

[15] G. Corcella, I. Knowles, G. Marchesini, S. Moretti, K. Odagiri, et al., *HERWIG 6.5 release note*, hep-ph/0210213 [INSPIRE].

[16] A. van Hameren, C. Papadopoulos and R. Pittau, *Automated one-loop calculations: a proof of concept*, *JHEP* **09** (2009) 106 [arXiv:0903.4665] [INSPIRE].

[17] M. Czakon, C. Papadopoulos and M. Worek, *Polarizing the dipoles*, *JHEP* **08** (2009) 085 [arXiv:0905.0883] [INSPIRE].

[18] S. Frixione, Z. Kunszt and A. Signer, *Three jet cross-sections to next-to-leading order*, *Nucl. Phys.* **B 467** (1996) 399 [hep-ph/9512328] [INSPIRE].

[19] J.M. Campbell and R. Ellis, *MCFM for the Tevatron and the LHC*, *Nucl. Phys. Proc. Suppl.* **205-206** (2010) 10 [arXiv:1007.3492] [INSPIRE].

[20] J.M. Campbell, R. Ellis and C. Williams, *MCFM web page*, http://mcfm.fnal.gov.

[21] M. Whalley, D. Bourilkov and R. Group, *The Les Houches accord PDFs (LHAPDF) and LHAGLUE*, hep-ph/0508110 [INSPIRE].

[22] Particle Data Group collaboration, K. Nakamura et al., *Review of particle physics*, *J. Phys.* **G 37** (2010) 075021 [INSPIRE].

[23] O. Latunde-Dada, S. Gieseke and B. Webber, *A positive-weight next-to-leading-order Monte Carlo for e^+e^- annihilation to hadrons*, *JHEP* **02** (2007) 051 [hep-ph/0612281] [INSPIRE].

[24] M. Cacciari, G.P. Salam and G. Soyez, *The $\bar{k}_t$ jet clustering algorithm*, *JHEP* **04** (2008) 063 [arXiv:0802.1189] [INSPIRE].

[25] M. Cacciari, G.P. Salam and G. Soyez, *FastJet user manual*, *Eur. Phys. J.* **C 72** (2012) 1896 [arXiv:1111.6097] [INSPIRE].

JHEP11(2012)056